Journal of Neurochemistry

JOURNAL OF NEUROCHEMISTRY | 2011 | 118 | 546–557

doi: 10.1111/j.1471-4159.2011.07336.x

ORIGINAL ARTICLE

Endogenous presynaptic nitric oxide supports an anterograde signaling in the central nervous system

Adriana Fernández-Alvarez,* Leonel Gómez-Sena,† María Gabriela Fabbiani,* Ruben Budelli† and Verónica Abudara*

*Laboratorio de Comunicación Celular, Departamento de Fisiología, Facultad de Medicina, Universidad de la República, General Flores 2125 Montevideo 11800, Uruguay

†Sección Biomatemáticas, Instituto de Biología, Facultad de Ciencias, Universidad de la República, Iguá 4225, Montevideo 11400, Uruguay

Abstract

The source size and density determine the extent of nitric oxide (NO) diffusion which critically influences NO signaling. In the brain, NO released from postsynaptic somas following NMDA-mediated activation of neuronal nitric oxide synthase (nNOS) retrogradely affects smaller presynaptic targets. By contrast, in guinea pig trigeminal motor nucleus (TMN), NO is produced presynaptically by tiny and disperse nNOS-containing terminals that innervate large nNOS-negative motoneurons expressing the soluble guanylyl-cyclase (sGC); consequently, it is uncertain whether endogenous NO supports an anterograde signaling between pre-motor terminals and postsynaptic trigeminal motoneurons. In retrogradely labeled motoneurons, we indirectly monitored NO using triazolofluorescein (DAF-2T) fluorescence, and evaluated sGC activity by confocal cGMP immunofluorescence. Multiple fibers stimulation enhanced NO content and cGMP immunofluorescence into numerous nNOS-negative motoneurons; NOS inhibitors prevented depolarization-induced effects, whereas NO donors mimicked them. Enhance of cGMP immunofluorescence required extracellular Ca^{2+}, a nNOS-physiological activator, and was prevented by inhibiting sGC, silencing neuronal activity or impeding NO diffusion. In conclusion, NO released presynaptically from multiple cooperative tiny fibers attains concentrations sufficient to activate sGC in many motoneurons despite of the low source/target size ratio and source dispersion; thus, endogenous NO is an effective anterograde neuromodulator. By adjusting nNOS activation, presynaptic Ca^{2+} might modulate the NO diffusion field in the TMN.

Keywords: anterograde transmission, cGMP, diffusion, motoneurons, nitric oxide, volume transmission.

J. Neurochem. (2011) **118**, 546–557.

The size of nitrergic sources critically determines the extent of NO diffusion (Lancaster 1994, 1997; Wood and Garthwaite 1994; Philippides *et al.* 2000, 2005) and consequently the NO spatial signaling capacity. Mathematical models predict that, the smaller the diameter of a single source, the lower the amount of produced NO and the lesser its diffusion distance (Philippides *et al.* 2000, 2005). Density of sources also determines the NO signaling efficiency; cooperation between many scattered fibers of low single efficacy can generate an extensive, strong, and homogenous volume signal (Philippides *et al.* 2005).

Received December 10, 2010; revised manuscript received May 23, 2011; accepted May 26, 2011.

Address correspondence and reprint requests to Dr Adriana Fernández-Alvarez and Dr Verónica Abudara, Departamento de Fisiología, Facultad de Medicina, General Flores 2125 Montevideo 11800, Uruguay.
E-mails: afernan@fmed.edu.uy and abudara@fmed.edu.uy

Abbreviations used: ACSF, artificial cerebrospinal fluid; CM-DiI, chlormethylbenzamido-1, 1 dioctadecyl-3, 3, 3′, 3′-tetramethylindocarbocyamine; c-PTIO, 2-(4-carboxyphenyl)-4,4,5,5-tetramethylimidazoline-1-oxyl-3-oxide, potassium salt; DAF-2DA, 4, 5-diaminofluorescein diacetate; DAF-2T, triazolofluorescein; DETA/NO, diethylenetriamine/nitric oxide adduct 2,2′-(hydroxynitrosohydrazono)bis-ethanimine; L-NAME hydrochloride, N^G-nitro-L-arginine-methyl ester.HCl; L-VNIO, vinyl-L-NIO, N^5-(1-imino-3-butenyl)-L-ornithine; MB, methylene blue; nNOS, neuronal nitric oxide synthase; NO, nitric oxide; ODQ, H-[1,2,4] oxadiazolo[4,3-a]quinoxalin-1-one; PBS, phosphate-buffered saline; PBST, PBS containing 0.1% Triton X-100; RH, rheobase; sGC, soluble guanylyl-cyclase; TMN, guinea pig trigeminal motor nucleus; TTX, tetrodotoxin; VGCCs, voltage-gated Ca^{2+} channels; ω-ctx-MVIIC, ω-conotoxin MVIIC.

Since NO diffuses through lipid and aqueous media (Denicola *et al.* 1996; Moller *et al.* 2005), it is released from any nNOS-containing compartment (Wiklund *et al.* 1997); then NO propagates in multiple directions according to concentration gradients (Lancaster 1994, 1997). In the brain, NO is typically produced by postsynaptic nNOS-expressing somas (10–100 μm diameter) following NMDA receptor-activation. Postsynaptically released NO modulates presynaptic terminals (0.1–5 μm diameter) acting as a retrograde messenger (Schuman and Madison 1994; Tao and Poo 2001); yet NO may act both pre- and postsynaptically (Garthwaite 2008). The high size ratio between postsynaptic sources and presynaptic targets guarantees that the NO field includes various subcellular/cellular targets as expected for a volume transmitter (Bredt and Snyder 1992; Zoli *et al.* 1998). Moreover, since postsynaptic nNOS and NMDA receptor are physically linked through the density protein PSD-95 (Christopherson *et al.* 1999), the NMDA receptor-mediated Ca^{2+} influx effectively stimulates the Ca^{2+}-dependent nNOS.

In contrast, the function of presynaptically released NO in the CNS has been far less studied; an explicit role has been reported in mammals (Mariño and Cudeiro 2003; Okada *et al.* 2004; West and Grace 2004) and invertebrates (Park *et al.* 1998). Accordingly, a role for presynaptic NO as anterograde neuromodulator of trigeminal (Abudara *et al.* 2002) and hypoglossal (Montero *et al.* 2008) motoneurons has been reported. At the TMN, nNOS is exclusively expressed by tiny (0.6–1.6 μm diameter) and disperse (2–30 μm separation) pre-motor fibers and bouton-like terminals closely associated to motor nNOS-negative somas (20–60 μm diameter) and dendrites (Abudara *et al.* 2002).

Trigeminal motoneurons contain the NO-molecular target, the sGC (Furuyama *et al*. 1993) and their excitability is modulated by exogenously applied NO donors through sGC activation (Abudara *et al.* 2002; see Montero *et al.* 2008 for hypoglossal motoneurons). We therefore hypothesized that endogenous NO produced by pre-motor nNOS-expressing fibers should signal postsynaptic trigeminal motoneurons. Nevertheless, since in the TMN the source/target size ratio is low and sources are scattered whether NO released from fibers effectively affects trigeminal motoneurons physiology is uncertain. The aim of this study was to determine that endogenous NO supports an anterograde transmission between tiny nitrergic fibers and large postsynaptic motoneurons in the TMN. In trigeminal motoneurons retrogradely labeled with chlormethylbenzamido-1, 1 dioctadecyl-3, 3, 3′, 3′-tetramethylindocarbocyamine (CM-DiI), we indirectly monitored intracellular NO with the fluorescent marker DAF-2T and sensed sGC activity by cGMP immunostaining during stimulation of multiple fibers. We demonstrate here that small sources, acting cooperatively, generate sufficient endogenous NO to recruit many large motoneurons at concentrations adequate to activate their sGC. We propose that, by adjusting nNOS activation, presynaptic Ca^{2+} that regulates classical neurotransmission would modulate the amount of produced NO at pre-motor fibers, and consequently, the extension of the NO volume influence in a cluster of motoneurons.

Materials and methods

Experimental procedures were conducted in accord with the National Research Council Guide for the Care and Use of Laboratory Animals (7th edition, Natural Academy Press, Washington, DC, 1996). The experimental protocol was approved by the Commission of Animal Experimentation (Facultad de Medicina – UDELAR). All efforts were made to minimize the number of animals used and their suffering.

Retrograde labeling of trigeminal motoneurons

Trigeminal motoneurons were identified using the non-cytotoxic fluorofore dye CM-DiI (Molecular Probes Inc., Eugene, OR, USA) as a retrograde tracer (Honig and Hume 1989). Guinea pigs were anesthetized with sodium pentobarbital (35 mg/kg weight intraperitoneal); the skin was incised to expose masseter muscles. CM-DiI (0.08% in 95% ethanol, total volume 12 μL) was injected into muscles. Animals recovered for a period of 7–14 days, allowing CM-DiI transport to trigeminal motoneurons in the TMN.

Preparation of guinea pig brain stem slices

Coronal living slices were obtained as described (Abudara *et al.* 2002). Guinea pigs (14–21 days old; 180–220 g/weight; 91 animals) were decapitated. Following craniotomy, the cerebellum was aspirated and the brain stem rapidly removed and placed in ice-cold artificial cerebrospinal fluid (ACSF) equilibrated with 95% O_2–5% CO_2. The brain stem was then glued to the platform of a vibroslicer chamber. Coronal slices (200–400 μm thick) containing the TMN were cut and transferred to a holding chamber where they rested on a nylon mesh, submerged in ACSF at 25°C for a stabilization period of at least 30 min.

Monitoring intracellular NO in living slices loaded with the indirect indicator 4, 5-diaminofluorescein diacetate (DAF-2DA)

Production and diffusion of NO were indirectly detected with high temporal and anatomical precision using the NO indicator and membrane-permeable DAF-2DA (Calbiochem, La Jolla, CA, USA) by microscopic visualization of DAF-2T fluorescence (Kojima *et al.* 1998a; Brown *et al.* 1999; Okada *et al.* 2004). Living slices (200 μm thick) were immersed in 5-μM DAF-2DA in ACSF equilibrated with 95% O_2–5% CO_2, for 30 min at 25°C. To minimize autofluorescence errors (Leikert *et al.* 2001), we have used a lower concentration of DAF-2DA (almost 50 %) than that previously reported in brain slices (Brown *et al.* 1999; Okada *et al.* 2004). After the incubation period, slices were rinsed twice in fresh ACSF. After loading, intracellular DAF-2DA is hydrolyzed by cytosolic esterases to yield DAF-2 which is non-permeable to cell membranes. In the presence of O_2, NO first forms NO_2 and then N_2O_3 which in turn irreversibly reacts with DAF-2 to yield the highly fluorescent compound DAF-2T

(Kojima *et al.* 1998a). Emitted fluorescence rises as a consequence of increases in the concentration of intracellular NO. NO_2 formation in biological solutions is a slow reaction (Beckman and Koppenol 1996), which imposes a limiting step in the velocity of the detection method. Caveats must be taken into account when interpreting this probe data (von Bohlen und Halbach 2003; Wardman 2007; Hall and Garthwaite 2009). It has been previously reported that ascorbic and dehydroascorbic acids react with DAF-2 and generate a DAF-2T-like fluorescence (Zhang *et al.* 2002). As well, in the presence of NO, intense light exposure (Broillet *et al.* 2001), UV illumination (Rodríguez *et al.* 2005), and DAF-2 oxidation (Espey *et al.* 2002; Jourd'heuil 2002) can enhance DAF-2T fluorescence. In this sense, to determine whether increases in DAF-2T fluorescence corresponded to increases in NO content, we treated preloaded slices with the NO donor diethylenetriamine/nitric oxide adduct 2,2′-(hydroxynitrosohydrazono)bis-ethanimine (DETA/NO), which spontaneously releases NO in solution and prevented high-$[K^+]_0$-induced fluorescence with the NOS blocker N^G-nitro-L-arginine-methyl ester.HCl (L-NAME hydrochloride; see 'Results'). L-NAME was added to the bath before loading slices with DAF-2DA. In the chamber perfusate, 2 mM DETA/NO is released with a flux of 1.54 μM/min as determined by spectrophotometry (Abudara *et al.* 2002).

Imaging system: analysis of DAF-2T fluorescence variations

Variations in NO content into trigeminal motoneurons were indirectly monitored by either time-lapse or stationary measurements of DAF-2T fluorescence intensity. For time-lapse experiments, the loaded slice was held on the lower surface of a coverslip fixed to a flow-through chamber that was mounted on the stage of an epifluorescent microscope (Nikon Optiphot; Nikon Inc., Melville, NY, USA). To identify retrogradely labeled motoneurons, slices were illuminated by a fluorescent light source *via* a filter set appropriate for CM-DiI (excitation wavelength 510–560 nm, emission wavelength 590 nm). After, the same field was illuminated by a fluorescent light source *via* a filter set for DAF-2T detection (excitation wavelength: 450–490 nm; emission wavelength: 520 nm). Objectives (10×, 20×, and 40×) were used. Photomicrographs were acquired by a digital camera (Kodak DC 290; Eastman Kodak Company, Rochester, NY, USA) attached to the microscope. For DAF-2T fluorescence processing, time-lapse measurements of fluorescence signals were recorded (every 30 s; exposure time = 0.5 s). Microscope and camera settings remained unchanged. Series of captured images were analyzed with an image program. The fluorescence intensity (F) for identified motoneurons in every image was measured in arbitrary units with a home-made program. The DAF-2 auto-fluorescence was subtracted from the total fluorescence. The ratio between F and F_0 (the initial fluorescence intensity at time = 0 min) was plotted versus time. The fluorescence values corresponding to the first ten photographs were discarded to avoid *bias* introduced by spurious peaks that may occur previous to the arrival of high-$[K^+]$ to the slice. We only considered peaks larger than 5% of basal fluorescence value. For stationary measurements of DAF-2T fluorescence, after maneuvers, slices were fixed overnight at 4°C in buffered 4% formaldehyde (pH 7.4), washed in phosphate-buffered saline (PBS) 0.1 M (pH 7.4), mounted in glycerol, and examined using a confocal microscope.

Electrophysiological recordings

Brain stem slices (400 μm thick) were used for intracellular recordings as described (Abudara *et al.* 2002). Slices containing the TMN are continuously perfused in a recording chamber (0.8–1 mL/min; ACSF bubbled with 95% O_2–5% CO_2) mounted on the stage of a microscope (Olympus CK2, Tokyo, Japan). Motoneurons were impaled with glass micropipettes (3 M KCl; 50–100 MΩ resistance; AM-Systems 6020, Sequim, WA, USA) pulled with a Brown-Fleming P-87 puller (Sutter Instrument Company, Novato, CA, USA). The microelectrode was connected to a bridge mode intracellular amplifier (Dagan model 8100; Dagan Corporation, Minneapolis, MN, USA) and lowered by a hydraulic micromanipulator (WR-6; Narishighe Scientific Instrument Lab., Tokyo, Japan). Electrical pulses (0.1–1 nA; 50 ms) were delivered through recording electrodes. Rheobase (RH) was the minimum stimulus intensity of a 50 ms intracellular depolarizing pulse that elicited an action potential.

Treatment of slices: solutions and drugs

Slices were either perfused (1 mL/min) or incubated with ACSF equilibrated with 95% O_2–5% CO_2. The ACSF solution contained (in mM): NaCl, 130; KCl, 3.0; $CaCl_2$, 2.4; $MgSO_4$, 1.3; $NaHCO_3$, 20; KH_2PO_4, 1.25; D-glucose, 10. Depolarization was accomplished with a modified extracellular ACSF solution (high-$[K^+]_0$; 13–30 min) in which KCl was increased to 43–60 mM by isosmolar substitution with NaCl.

In blocking experiments, slices were treated prior to and during exposure to high-$[K^+]_0$ with one of the following blockers: L-NAME hydrochloride (0.3–1 mM); vinyl-L-NIO, N^5-(1-imino-3-butenyl)-L-vornithine (L-VNIO; 1 μM); 2-(4-carboxyphenyl)-4,4,5,5-tetramethylimidazoline-1-oxyl-3-oxide, potassium salt (c-PTIO; 30 μM); H-[1,2,4] oxadiazolo[4,3-a]quinoxalin-1-one (ODQ; 5–10 μM); tetrodotoxin (TTX; 1 μM), and ω-conotoxin MVIIC (ω-ctx-MVIIC; 1 μM). To determine the effect of extracellular Ca^{2+} on high-$[K^+]_0$-induced cGMP immunostaining, slices were incubated 20 min prior to and during high-$[K^+]_0$ exposure in a $[Ca^{2+}]_0$-deficient high-$[K^+]_0$ ACSF solution whose composition consisted in the high-$[KCl]_0$ ACSF solution with the following modifications: 0.2 mM Ca^{2+}, 4 mM Mg^{2+}, and addition of EGTA (2 mM).

In blocking electrophysiological experiments, methylene-blue (MB; 100 μM), was dissolved in the ACSF solution (equilibrated with 95% O_2–5% CO_2).

The DETA/NO (2 mM) and NMDA (10 μM) were dissolved in the ACSF solution.

L-NAME and L-VNIO were obtained from Alexis (Plymouth Meeting, PA, USA); c-PTIO, ODQ, TTX, ω-ctx-MVIIC, and NMDA from Tocris (Ellisville, MO, USA); and EGTA, MB, and DETA/NO from Sigma (St. Louis, MO, USA).

cGMP immunohistochemistry

After overnight fixation at 4°C in buffered 4% formaldehyde (pH 7.4), slices were washed three times for 20 min in PBS 0.1 M (pH 7.4), and kept cryoprotected for 24 h in 30% sucrose in PBS. Afterwards, slices were immersed in tissue freezing medium (Jung; Leica microsystems, Nussloch, Germany), frozen, and cut in sections (30 μm thick) using a cryostat. Sections were placed in a multiwell dish and washed three times for 20 min in PBS. Afterwards, sections were blocked 1 h in 2% bovine serum albumin

diluted in PBS. After three rinses in PBS, they were incubated for 24 h at 4°C with primary antibody polyclonal Rabbit anti-cGMP serum (1 : 1000, #AB303; Chemicon, Temecula, CA, USA) diluted in PBS containing 0.1% Triton X-100 (PBST). The day after, sections were washed three times for 10 min in PBST and incubated for 90 min with secondary antibody (1 : 1000, Donkey anti-rabbit Alexa 488; Molecular Probes) diluted in PBST. Some sections were incubated omitting primary and/or secondary antibodies as negative controls. After that, sections where washed in PBS, mounted in glycerol, and examined using a confocal microscope.

Confocal microscopy

Images were observed with confocal microscopy (FV 300 Olympus, Tokyo, Japan) at 20× (stationary DAF-2T fluorescence) or 40× (cGMP immunohistofluorescence). Consecutive confocal images taken at 1–5 μm intervals were acquired sequentially with two lasers, Ar–Ion (488 nm) and Green He–Ne (543 nm) using the Olympus Fluoview software. Microscope and camera settings remained the same in experiments in which comparisons were made. Fluorescence was evaluated in arbitrary units with image processing software Image J (NIH, Bethesda, MD, USA). Fluorescence intensity was calculated as the difference ($F - F_0$) between the fluorescence (F) from motoneurons and the background fluorescence level (F_0) measured where no labeled cells were detected. The ratio between $F_{treatment}$ and $F_{control}$ was plotted for each treatment.

Statistics

Values are presented as mean values ± SEM; n expresses the number of motoneurons. The non-parametric two-tailed Mann–Whitney U-test was used to compare the effects of different treatments because data was not normally distributed. In dynamic (time-lapse fluorescent) experiments, to compare the relations between the maximum amplitude and the rising slope of the fluorescence intensity curves obtained under different treatments, we first checked that the linear regression gave good fits to sets of data. Then, a standard analysis of covariance was applied. For all experiments, the level of significance was set at $p < 0.05$. Statistics were performed using the SPSS 15.0 for Windows software (Montevideo, Uruguay). Graphics were prepared using SPSS 15.0 for Windows and Corel DrawX3 (2005).

Results

Trigeminal motoneurons can be identified in living brain stem slices by CM-DiI retrograde labeling

Trigeminal motoneurons were successfully identified in guinea pig living slices by CM-DiI-retrograde labeling (Fig. 1). At higher magnification, cell bodies exhibited strong and granular fluorescence typical of carbocyanine fluorophore staining (Fig. 1b). CM-DiI labeled perikarya and initial segments of dendritic processes, remaining confined to the cytoplasm. Motoneurons showed trapezoid and multipolar somas (diameters range: 20–60 μm, average: 35 μm; $n = 82$).

CM-DiI-identified cells matched TMN location (Uemura-Sumi *et al.* 1982) and their morphology agreed with previous

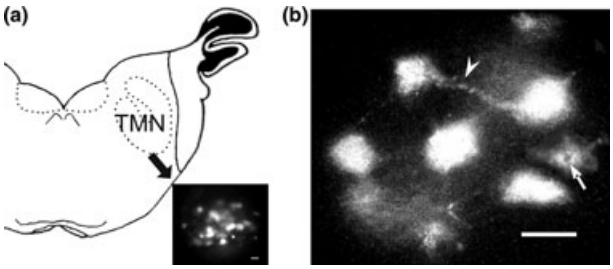

Fig. 1 Identification of trigeminal motoneurons by CM-DiI retrograde labeling in living slices. (a) Scheme of guinea pig coronal brainstem slice indicating TMN location; inset: low magnification view of fluorescent CM-DiI-retrogradely labeled trigeminal motor neurons. (b) High magnification fluorescent image shows TMN motoneurons from a different living slice (200 μm thick). Arrowhead: one discernible dendritic process; arrow: non-fluorescent cell nucleus. Scale bars: 50 μm in (a, inset) and (b).

description of trigeminal motoneurons (Shigenaga *et al.* 1988). Therefore, we discarded a potential labeling of non-motoneuronal structures, such as interneurons and glia because of fluorophore diffusion from sectioned cell bodies (Honig and Hume 1989). As false-negative results can be found with retrograde fluorescent tracers, some CM-DiI-negative structures could also correspond to motoneuronal components.

Endogenous NO is found in nNOS-free trigeminal motoneurons under basal conditions

Localized DAF-2T fluorescence was evident in the absence of stimulation (Fig. 2a). Three basal patterns were identified (69 slices). In 38% of slices, DAF-2T fluorescence was not detected (pattern I, Fig. 2a, i′ and i″). In 17% of slices, DAF-2T-positive/CM-DiI-negative fiber-like and granular structures were observed in apposition to CM-DiI-positive motoneuron somas (pattern II, Fig. 2a, ii′ and ii″). Since these NO-containing fiber-like structures reminded the morphology and size of nNOS-expressing pre-motor fibers and their anatomical rapport with TMN motoneurons described in fixed sections (Abudara *et al.* 2002), and because the NOS inhibitor L-NAME (Alderton *et al.* 2001) decreased their visualization (see next), they might represent NO-producing fibers. Finally, the remaining 45% of slices exhibited DAF-2T-labeled somas (pattern III, Fig. 2a, iii′ and iii″). Since neither trigeminal motoneurons nor somas in the TMN express either nNOS or NADPH-diaphorase activity (Abudara *et al.* 2002), we concluded that NO contained within nNOS-negative motoneurons (Fig. 2a, iii″) was released from non-motoneuronal sources, diffused and entered into these motoneurons. L-NAME (0.3–1 mM), decreased patterns II plus III from 62% to 25% suggesting that endogenous NO was basally produced.

Most trigeminal motoneurons were DAF-2T-negative under basal conditions; nevertheless, when motoneurons

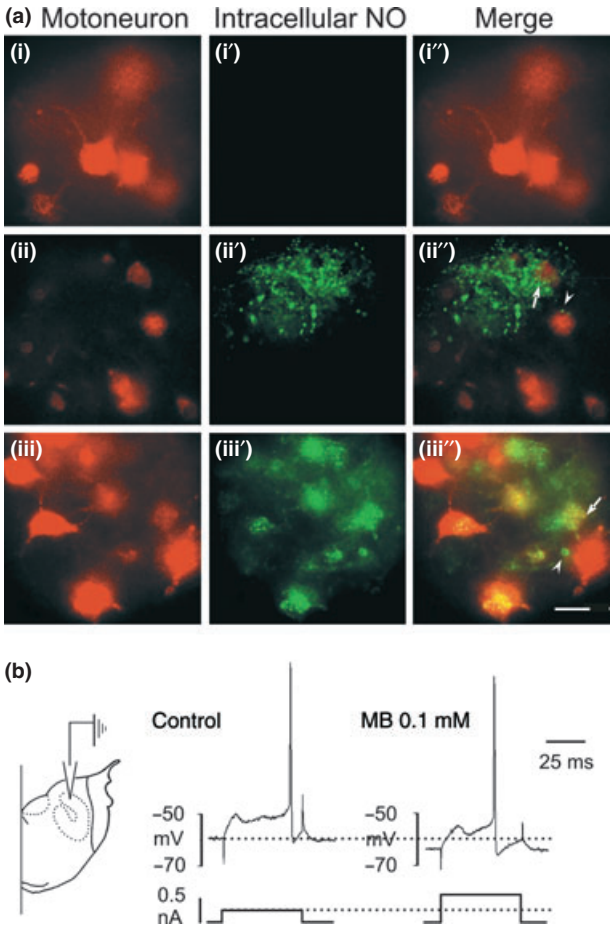

Fig. 2 Endogenous NO in the TMN under basal conditions: production, diffusion and biological effects. (a) Distribution of the DAF-2T fluorescence in the TMN under basal conditions in guinea pig living slices. Fluorescent images in each line (i, i′, i″; ii, ii′, ii″, and iii, iii′, iii″) correspond to the same field; first column: CM-DiI (red); second column: DAF-2T (green); third column: merged or colocalization of both dyes (yellow) (69 slices; 18 animals). Three DAF-2T fluorescence patterns were determined: (1) DAF-2T-positive structures could not be detected (i′, i″); (2) DAF-2T-positive/CM-DiI-negative fluorescent fiber-like and granular structures (ii′, ii″), and (3) DAF-2T-positive somas of CM-DiI-positive trigeminal motoneurons (iii′, iii″). Arrow in (ii″): DAF-2T fiber-like structures surround a DAF-2T-negative motoneuron. Arrowheads in (ii″) and (iii″) indicate CM-DiI-negative/DAF-2T-positive processes adjacent to DAF-2T-negative motoneurons. Arrow in (iii″): DAF-2T fluorescent motoneuron is proximate to a DAF-2T-negative motoneuron. Scale bars: 50 μm. (b) Electrophysiological intracellular recordings of a trigeminal motor neuron in control and after MB perfusion (100 μM). The intensity of the depolarizing current pulse was adjusted to the threshold level in every trial. MB hyperpolarized the neuron from −59 to −64 mV and increased its rheobase from 0.39 to 0.57 nA (three cells, three slices, three animals). Note the decrease in the action potential onset delay under MB.

are reached by NO (Fig. 2a, iii″), they might be modulated by basal NO. As exemplified in Fig. 2(b), in the absence of stimulation, MB (100 μM), a non-specific sGC, and NOS inhibitor (Hobbs 1997) hyperpolarized motoneurons and increased their RH. This result suggests that, at least *in vitro*, the spontaneous release of NO modulates the electrophysiological properties of motoneurons. In agreement, NO donors depolarize and decrease the RH of TMN motoneurons in guinea pig brain stem slices (Abudara *et al.* 2002).

Depolarization enhances the content of endogenous NO in postsynaptic trigeminal motoneurons

In neurons, NO is produced following the activity-dependent entry of Ca^{2+} which binds to calmodulin and activates nNOS (Bredt and Snyder 1990). In the TMN, depolarization is expected to open voltage-gated Ca^{2+} channels (VGCCs) at nitrergic terminals allowing Ca^{2+} influx and nNOS activation. Thereby we tested the effect of depolarization on NO generation in DAF-2DA loaded slices. We used a depolarizing high-$[K^+]_0$ solution to analyze a potential cooperation between several tiny nNOS-expressing TMN fibers and because these fibers form a fine presynaptic plexus that impede to selectively stimulate individual nitrergic axons (or bundles).

High-$[K^+]_0$ significantly increased DAF-2T fluorescence in identified motoneurons suggesting that depolarization increases motoneuron NO content (Figs 3 and 4). Time-lapse variations of DAF-2T fluorescence signals were evaluated prior to and during perfusion with high-$[K^+]_0$. Motoneuronal structures retrogradely labeled with CM-DiI were identified in a selected field (Fig. 3c inset) which in control was DAF-2T-negative (Fig. 3a, 0 min). Initially (0.5–3 min, Fig. 3a), high-$[K^+]_0$ induced a simultaneous and extensive increase of the DAF-2T signal but after, strong DAF-2T fluorescence was concentrated at discrete zones that then delimited nNOS-negative motoneurons initially not labeled with DAF-2T (3–18 min, Fig. 3a). This suggests that non-motoneuronal sources supplied endogenous NO which then diffused and invaded motoneurons (see DAF-2T-positive motoneurons in yellow, Fig. 3b). For each identified motoneuron, DAF-2T fluorescence changes were plotted (Fig. 3c; curves). The first component of the biphasic DAF-2T fluorescence curves (5 min; Fig. 3c) might correspond to simultaneous NO synthesis in many nitrergic fibers (scattered fluorescence, Fig. 3a and b). The second component (9–19 min; Fig. 3c) showing higher intensities might correlate with extramotoneuronal NO production and further accumulation into cells (DAF-2T-positive motoneurons, Fig. 3a and b). Delays in the range of several minutes have been reported when detecting DAF-2T signals (Kojima *et al.* 1998b, 2001; Okada *et al.* 2004); indeed, the time required to yield DAF-2T includes intermediate reaction steps (see 'Materials and methods'). Besides, nNOS availability, innervation density, source size and distribution, NO dissipation and scavenging and proximity of motoneurons to blood vessels determine NO delivery and thus, impact on delays to attain DAF-2T signals. In TMN, fineness and separation between fibers might have delayed achieving an effective NO signal (Philippides *et al.* 2005). As

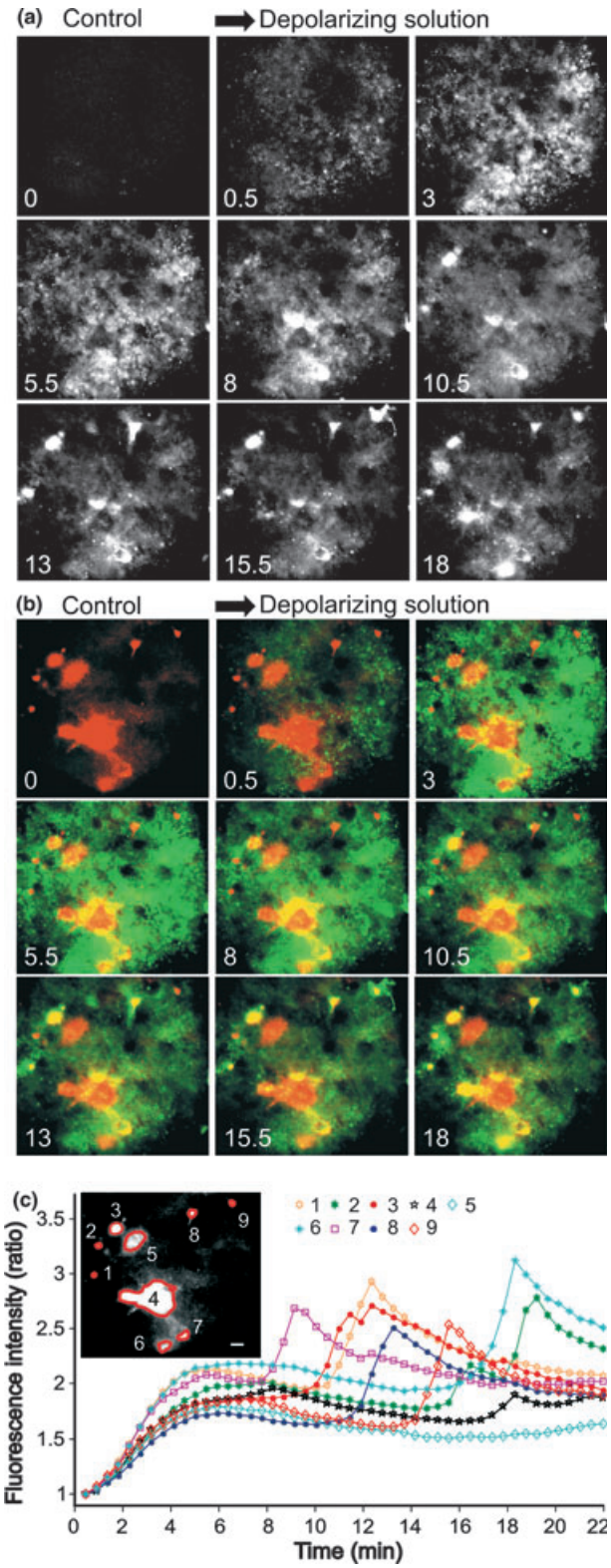

Fig. 3 High-$[K^+]_0$ induces a rise of endogenous levels of NO in nNOS-negative trigeminal motoneurons. (a) Time-lapse recordings of DAF-2T fluorescence variations in trigeminal motoneurons from a living slice during high-$[K^+]_0$. The selected field does not exhibit DAF-2T fluorescence under basal conditions (control), however, depolarization induces it. The time (min) elapsed after high-$[K^+]_0$ application is indicated in each picture. Initially (0.5–3 min), a widespread fluorescence increase is detected; afterwards (3–8 min), bright fluorescence confines to discrete zones that then (8–18 min) delimit motoneuronal structures (DAF-2T-positive motoneurons). (b) Color representation of the experiment shown in (a). Color images of the sequence recorded in (a) were superimposed onto the color image of (c) inset showing CM-DiI-labeled TMN motoneurons for the same field. Red: CM-DiI-labeled motoneurons; green: DAF-2T-labeled intracellular NO; yellow: co-localized CM-DiI and DAF-2T labeling evidencing intramotoneuronal NO. (c) Time course of the DAF-2T fluorescence signal from the same experiment. The fluorescence signal is expressed as the ratio between the fluorescence intensity at every time indicated in the curve and the initial fluorescence intensity (i.e. at 0 min) for each identified motoneuron. Inset: red contours display motoneuronal structures identified by CM-DiI retrograde labeling ($n = 9$). Note that maximum curves in (c) and emerging yellow structures in (b) are temporally correlated. Scale bars in (a), (b), and (c): 20 μm.

well, the effectiveness of the VGCCs-mediated Ca^{2+} influx to activate intraterminal nNOS is unknown.

Typically, DAF-2T-fluorescent motoneurons were found neither under control (physiological solution) nor under NOS-inhibited conditions (L-NAME + high-[K+]; Fig. 4a, first and second graphs respectively).

The maximum DAF-2T fluorescence ratios for identified motoneurons were grouped in classes (bin size: 0.5; range: 1–6) and plotted in frequency histograms for different experimental conditions (Fig. 4b, insets). Histograms for control and L-NAME + high-$[K^+]_0$ experiments show that maximum DAF-2T fluorescence ratios were mostly included in 1 and 1.5 classes. These peaks may correspond mainly to random variations. Under high-$[K^+]_0$, we registered values included in categories larger than 2 for DAF-2T-positive motoneurons (Fig. 4b insets). In contrast, amplitude ratios larger than 2 were recorded neither under control nor under L-NAME + high-$[K^+]_0$ suggesting that the DAF-2T fluorescence specifically required intracellular NO: in control, the absence of depolarization prevented intraterminal $[Ca^{2+}]_i$ increases and consequently nNOS activation; under L-NAME, nNOS was competitively inhibited (Fig. 4b insets and Fig. 4a, first and second graphs, respectively).

Accumulated frequency curves for maximum DAF-2T fluorescence ratios show the main presence of DAF-2T-positive motoneurons under high-$[K^+]_0$ as compared with control and L-NAME experiments (Fig. 4b). Because trigeminal motoneurons are nNOS-negative, NO was supplied by non-motoneuronal sources and diffused toward these cells.

To validate DAF-2DA as a sensitive and specific NO sensor, we exposed DAF-2DA-preloaded slices to the NO-donor DETA/NO (2 mM) (Fig. 4). Typically DETA/NO (2 mM) induced an intense and simultaneous increase of the DAF-2T fluorescence which attained similar levels in identified motoneurons (Fig. 4a, third graph). Since pattern profiles for DAF-2T variations were similar for all tested

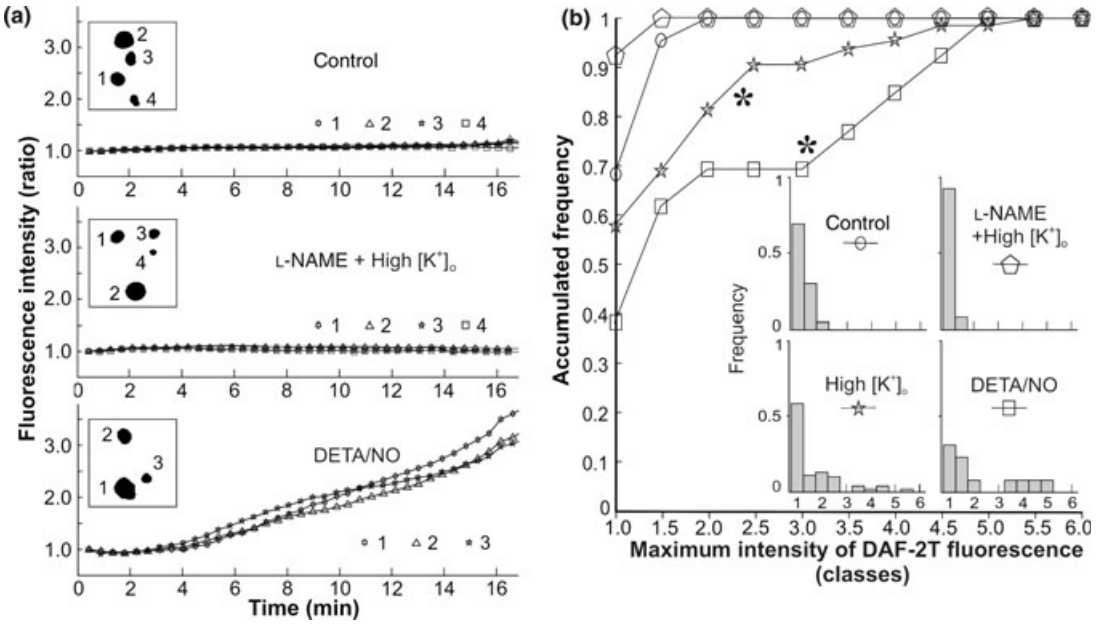

Fig. 4 DAF-2T-positive motoneurons are evoked by both endogenous (high-$[K^+]_0$–induced) and exogenous (NO donors) NO. (a) Typical examples show the temporal course of DAF-2T fluorescence intensity variations in TMN motoneurons during perfusion with, physiological solution ACSF (control), L-NAME + high-$[K^+]_0$, and DETA/NO. CM-DiI-identified motoneuronal structures are represented as black spots (insets). The fluorescence signal is expressed as in Fig. 3(c). (b) Frequency distributions for the maximum DAF-2T fluorescence intensities for identified motoneurons. Histograms in inset: frequency histograms of maximum values of DAF-2T fluorescent intensity (grouped in classes, bin: 0.5, range: 1–6), from slices subjected to different conditions: control (n = 62; 17 slices; six animals), high-$[K^+]_0$ (n = 95; 20 slices; 10 animals), L-NAME + high-$[K^+]_0$ (n = 15; seven slices; four animals), and DETA/NO (n = 15; six slices; four animals) experiments. Maximum intensities included in bins greater than 2 are only detected in histograms of high-$[K^+]_0$ and DETA/NO treated slices. Curves: accumulated frequency curves of maximum fluorescence intensities for slices treated with high-$[K^+]_0$ and DETA/NO exhibit increased motoneuronal content of NO as compared with control. The high-$[K^+]_0$ effect was blocked by L-NAME; L-NAME + high-$[K^+]_0$ curve did not differ from control. *$p < 0.05$, compared with the control curve.

cells, we discarded that heterogeneity in dye loading (Rodríguez *et al.* 2005) or a differential access to O_2 (Ledo *et al.* 2005) were highly distorting our recordings (O_2 is required to obtain DAF-2T fluorescence). As for high-$[K^+]_0$, slices treated with DETA/NO showed DAF-2T-positive motoneurons and maximum fluorescence ratios larger than 2 (Fig. 4b inset); indeed, accumulated frequency curves for maximum fluorescence ratios for DETA/NO and high-$[K^+]_0$ experiments were not significantly different ($p > 0.05$; Fig. 4b). To compare dynamics of NO increases, the rising slope of the temporal course of the DAF-2T fluorescence was plotted versus the maximum fluorescence intensity for high-$[K^+]_0$ and DETA/NO experiments; these parameters varied proportionally adjusting to straight lines. The relationship was steeper for high-$[K^+]_0$ than for DETA/NO trials (Fig. 5). This divergence might reflect differences in the mechanisms underlying NO supply under both circumstances: in our experiments, synthesis of NO by nNOS might be faster than NO released from NO donors. Also, the eventual generation of oxidative radicals might have oxidized DAF-2 to a free radical intermediate enhancing the fluorescence signal in TMN motoneurons upon depolarization (Espey *et al.* 2002; Jourd'heuil 2002) although, it has been reported that metabolic activity (Bredt 1999) but not high-$[K^+]_0$ (Bindokas *et al.* 1996) increases neuronal superoxide (O^{-2}) generation.

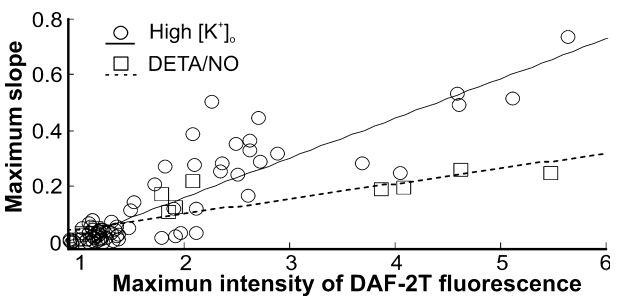

Fig. 5 Differential dynamics of intramotoneuronal NO increases between endogenously generated and exogenously applied NO. The maximum rising slope of the temporal course of DAF-2T fluorescence curves is plotted versus the maximum intensity fluorescence reached by each identified motoneuron for high-$[K^+]_0$ and DETA/NO experiments. Linear regression fits for each experimental group are superimposed to data. R^2 = 0.78 for high-$[K^+]_0$ (n = 75; 20 slices; 10 animals) and 0.77 for DETA/NO (n = 15; six slices; four animals); $p < 0.001$ (covariance test).

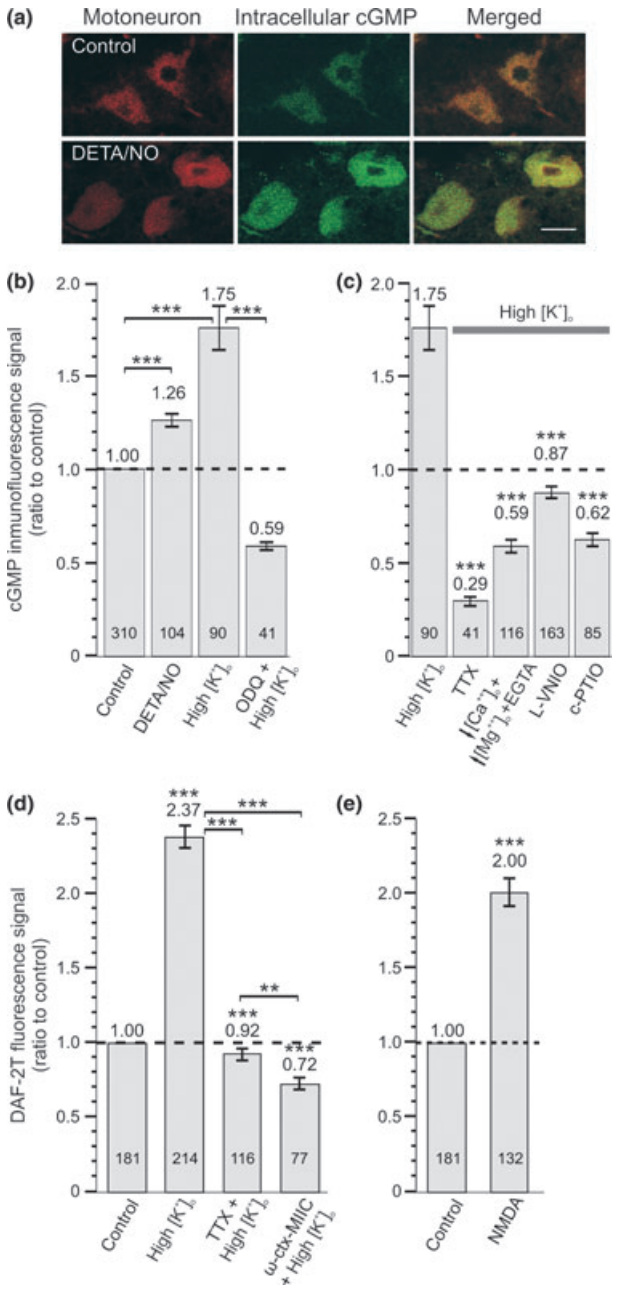

Fig. 6 Endogenous NO attains postsynaptic trigeminal motoneurons at effective biological concentrations by activating the sGC. (a) Fluorescent images of CM-DiI labeled motoneurons (red, first column) and anti-cGMP immunofluorescence (green, middle column) under control conditions (control) and upon administration of exogenous NO (DETA/NO). Both images (CM-DiI-labeled and anti-cGMP immunofluorescence) from the same slice (or condition) were superimposed (merged) to evidence intramotoneuronal cGMP (yellow, third column). (b) Endogenously generated (high-$[K^+]_0$) and exogenously applied NO (DETA/NO) increase cGMP synthesis through sGC activation. DETA/NO (five slices; five animals) and high-$[K^+]_0$ (four slices; four animals) increase motoneuronal cGMP immunofluorescence as compared with control (20 slices; 18 animals); the high-$[K^+]_0$ effect is totally prevented by pre-treatment with ODQ (5–10 μM) (four slices; four animals). (c) The high-$[K^+]_0$-induced cGMP inmunofluorescence (horizontal gray bar) is prevented by blocking neural transmission, impeding Ca^{2+} influx, NO production, and extracellular diffusion. Signal increase is completely prevented by TTX (1 μM) (four slices; three animals), low-$[Ca^{2+}]_0$ + high-$[Mg^{2+}]_0$ + EGTA (2 mM) (five slices; three animals), L-VNIO (1 μM) (eight slices; eight animals), or c-PTIO (30 μM) (five slices; four animals). ***$p < 0.001$ as compared with high-$[K^+]_0$. (d) Blocking neural transmission or presynaptic VGCCs prevent the high-$[K^+]_0$-induced DAF-2T fluorescence. High-$[K^+]_0$ + TTX (1 μM) (seven slices; six animals); high-$[K^+]_0$ + ω-ctx-MVIIC (1 μM) (six slices; six animals); high-$[K^+]_0$ (13 slices; 10 animals); control (12 slices; 10 animals); asterisks above mean values over bars indicate *p*-value as compared with control. (e) NMDA increases NO content in motoneurons. NMDA (10 μM) (eight slices; five animals); control as in (d). In graphs (b–e), the fluorescence signal value for treated motoneurons in A.U. was normalized to that for control cells; ratio means were plotted over bar graphs. **$p < 0.01$; ***$p < 0.001$; numbers in bars represent the number of cells. Scale bar in (a): 50 μm.

In any case, regardless of the difficulty to reconcile if DAF-2T fluorescence is linearly proportional to only free NO concentration, DAF-2T fluorescence increases in the TMN (i) required production of NO and (ii) reflected rises in the intracellular content of NO since DAF-2T fluorescence: (a) increased as the result of NO release by NO/donors and (b) was sensitive to the NOS inhibitor L-NAME.

Depolarization enhances the cGMP immunostaining signal in nNOS-negative sGC-expressing trigeminal motoneurons

According to results obtained by bioimaging, NO supplied by tiny nitrergic fibers is sufficient to reach trigeminal motoneurons. However, is the concentration of endogenous NO effective to modulate these cells? The main downstream effector of NO, the sGC, has been immunolocalized in TMN motoneurons where it mediates the effects of NO donors on motoneuronal excitability. Then, we determined whether both endogenously generated (high-$[K^+]_0$-induced NO) and exogenously applied (NO donors) NO entering into postsynaptic motoneurons could activate the sGC. We employed cGMP immunocytochemistry to evaluate and locate sites of sGC activity (De Vente *et al.* 1998) and as a functional evidence of an effective biological concentration of endogenous NO (Hall and Garthwaite 2009). Both DETA/NO (2 mM; 30 min; Fig. 6a, bottom panel, and Fig. 6b) and high-$[K^+]_0$ (Fig. 6b) increased cGMP immunostaining in CM-DiI-labeled motoneurons as compared with control. High-$[K^+]_0$ effect was attributed to an augmented sGC activity since the potent/specific sGC inhibitor ODQ (5–10 μM) completely prevented it (Fig. 6b). Moreover, this effect was also completely prevented by the nNOS blocker L-VNIO (see Fig. 6c); therefore neuronal endogenously synthesized NO-mediated high-$[K^+]_0$-induced cGMP labeling. These data indicate that either exogenous or endogenous NO effectively stimulates cGMP synthesis in TMN moto-

neurons. The fact that ODQ reduced cGMP labeling below control (Fig. 6b) suggests that basal synthesis of cGMP controls motoneuron physiology in agreement with data obtained in Fig. 2.

These findings support the concept that during depolarization (of nerve terminals), released NO that enters into trigeminal motoneurons is sufficient to activate the sGC promoting cGMP synthesis. We conclude that endogenous NO modulates postsynaptic motoneurons and mediates an effective anterograde transmission in the TMN.

The anterograde NO-mediated transmission in the TMN is activity-dependent and requires extracellular Ca^{2+}, activation of presynaptic nNOS and diffusion of NO

From a classical anterograde neurotransmission perspective, mechanisms coupling depolarization of nitrergic terminals to postsynaptic cGMP synthesis, include activation of voltage-regulated Na^+ channels in depolarized nitrergic fibers, Ca^{2+} influx through opened VGCCs, nNOS activation, production and diffusion of NO from pre-motor fibers, entry of NO into nNOS-free sGC-expressing motoneurons, and sGC activation. We then determined the pharmacological sensitivity of the high-$[K^+]_0$-induced cGMP signal to prevent those phases.

The voltage-gated Na^+-channel and action potential blocker TTX (1 μM) completely inhibited both high-$[K^+]_0$-induced cGMP immunostaining (Fig. 6c) and DAF-2T fluorescence (Fig. 6d) in TMN motoneurons suggesting that activation of voltage-gated Na^+ channels is a major component of NO-mediated transmission during evoked neuronal activity. TTX reduced both signals below control; this suggests an activity-dependent cGMP synthesis under basal conditions (in agreement with results of Fig. 2), probably because of spontaneous neural activity.

High-$[K^+]_0$-induced cGMP staining of motoneurons was prevented when slices were incubated in a $[Ca^{2+}]_0$-deficient ACSF solution that contained, low $[Ca^{2+}]$ (0.2 mM), EGTA (2 mM), a Ca^{2+} -chelating agent and high $[Mg^{2+}]$ (4 mM), a Ca^{2+}-channel blocker if used at high concentrations (Fig. 6c). Furthermore, ω-ctx-MVIIC (1 μM), an inhibitor of presynaptic N-, P-, and Q-type VGCCs, prevented high-$[K^+]_0$-induced DAF-2T fluorescence (Fig. 6d). Therefore, NO signaling requires the influx of external Ca^{2+} through presynaptic VGCCs.

L-NAME did not allow discerning which NOS iso-enzyme was activated. Therefore, we treated slices with L-VNIO (1 μM), a selective nNOS blocker (Alderton *et al.* 2001). L-VNIO abolished high-$[K^+]_0$-induced cGMP immunostaining evidencing its dependence on nNOS activation (Fig. 6c).

To determine that NO released from nitrergic terminals diffuses through the extracellular milieu to reach motoneurons, extracellular NO was scavenged with c-PTIO, a stable and water-soluble free radical that reacts stoichiometrically with NO. The c-PTIO (30 μM) potently inhibited depolarization-induced cGMP immunostaining demonstrating that NO responsible for the activation of motoneuronal sGC is supplied by non-motoneuronal sources (Fig. 6c).

Finally, application of the glutamate agonist NMDA (10 μM), which mediates Ca^{2+} influx, increased NO content in trigeminal motoneurons with a minor intensity than high-$[K^+]_0$ ($p < 0.01$; Fig. 6e).

In conclusion, results obtained support that, throughout TMN NO-mediated transmission, events coupling presynaptic depolarization to postsynaptic motoneuron modulation resemble those of a classical anterograde neurotransmission.

Discussion

Herein, we demonstrate that exposing TMN-containing slices to a high-$[K^+]_0$ solution enhances NO content and cGMP immunoreactivity in non-nNOS sGC-expressing trigeminal motoneurons (Figs 3, 4 and 6). These findings might be ascribed to (i) the evoked release of NO from tiny pre-motor nNOS-expressing fibers following Ca^{2+} entry through presynaptic VGCCs during neuronal activity that (ii) activated the Ca^{2+}-calmodulin regulated nNOS at nerve terminals leading to production of NO which then (iii) diffused from pre-motor fibers and entered into trigeminal motoneurons at effective biological concentrations, adequate (iv) to activate the sGC and increase intracellular cGMP. Also NO generated under basal conditions modulated TMN motoneurons excitability (Fig. 2). Our results evidence that in the TMN endogenously nNOS-triggered NO sustains, an anterograde signaling regardless of the important inequality between sources and targets sizes. Although NO diffusion is multidirectional, the term anterograde refers here to the directionality of nitrergic effects: NO released from pre-motor fibers modulates postsynaptic motoneurons activity.

In the TMN, the extent of NO signaling enables the recruitment of clusters of motoneurons

The NO concentration is highest at the source surface and decreases as NO diffuses away (Lancaster 1994, 1997; Philippides *et al.* 2005). The source size critically determines the production extent and diffusion dynamics of NO: the thinner the fiber is, the lower the surface concentration is attained and the sharper the last declines over distance (Philippides *et al.* 2005). As corollaries, we expect that, (i) differential activation of fibers with different sizes provides differential release of NO and (ii) the distance between sources and targets inversely relates to NO signaling strength (Park *et al.* 1998). Since most TMN nNOS-expressing fibers are fine (0.6–1.6 μm diameters) and proximate to motoneuron dendrites (Abudara *et al.* 2002), we hypothesized that a single fiber would produce an amount of NO sufficient to affect only adjacent dendrites. According to Philippides *et al.* (2005) modeling, for 1 μm diameter fibers, NO is predicted to attain the minimum concentration (5 nM) required to generate a DAF-2T signal (Kojima *et al.* 1998a) at 30–35 μm away

from surface; over larger distances, the probe would not sense NO; for thinner fibers, the threshold would be reached at minor distances. Herein, we found that numerous 50–60 μm diameter motoneuronal somas became DAF-2T-positive when multiple and disperse tiny NO-producing fibers were stimulated. We therefore concluded that NO produced by thin fibers should have cooperated (Philippides *et al.* 2005) to turn DAF-2T-positive the large somas of motoneurons (Fig. 3); this has *in vivo* implications because an action potential traveling through the axons of nNOS-expressing pre-motor neurons will evoke the diffusion of NO from multiple terminals toward a postsynaptic motoneuron. The concentration of NO required for sGC activation (effective biological NO concentration; Griffiths *et al.* 2003; Mo *et al.* 2004) is lower than the threshold for DAF-2T fluorescence detection (Kojima *et al.* 1998a); therefore, cGMP synthesis should take place at DAF-2T-positive structures cells; in agreement, various motoneurons also enhanced cGMP immunoreactivity following depolarization (Fig. 6).

Released NO might exert an excitatory effect on TMN motoneurons (Fig. 2b) by acting either directly on postsynaptic currents (Montero *et al.* 2008) or on the presynaptic release of neurotransmitters (Garthwaite 2008) which in turn would modulate motoneurons excitability. In the TMN, both mechanisms might take place; at trigeminal motoneurons, application of NO donors increased the hyperpolarization-activated cationic current (I_h) as well as the synaptic activity (Abudara *et al.* 2002).

Nitrergic sources in the TMN

At the guinea pig TMN, nNOS is exclusively detected in pre-motor fibers and bouton-like terminals (Abudara *et al.* 2002), then NO evoking the sGC- and nNOS-dependent cGMP synthesis (respectively, ODQ- and L-VNIO-sensitive components; Fig. 6b and c) was supplied by these fibers. That TMN motoneurons do not express nNOS is supported by the fact that they do not show either nNOS immunoreactivity or NADPH-diaphorase histochemical activity associated with nNOS (Hope *et al.* 1991; Abudara *et al.* 2002). Accordingly, rat trigeminal (Pose *et al.* 2011b) and hypoglossal (Montero *et al.* 2008) motoneurons also lack the molecular machinery to synthesize NO. Since scavenging extracellular NO inhibited high-$[K^+]_0$-evoked cGMP labeling (c-PTIO, Fig. 6c), then NO came from extramotoneuronal sources. Astrocytes expressing NOS (Murphy *et al.* 1993) are not good candidates as sources because constitutive NOS-containing somas were not identified in the TMN (Abudara *et al.* 2002). Inhibiting either the neural activity (TTX; Fig. 6c and d) or Ca^{2+} influx through presynaptic VGCCs ($[Ca^{2+}]_0$-deficient solution and ω-ctx-MVIIC; Fig. 6c and d) prevented both increased DAF-2T fluorescence and cGMP labeling. These findings support that depolarization invaded nNOS-containing terminals, opened presynaptic VGCCs allowing Ca^{2+} entry that consecutively triggered release of NO which then diffused and invaded motoneurons where it activated neuronal sGC.

Spatial segregation between pre-motor axo-terminal and somato-dendritic sources confers functional properties to NO signaling in the TMN

Somas of origin of TMN nitrergic fibers were identified in the ventromedial medullary reticular formation (Pose *et al.* 2005) and dorsomedial hypothalamic nucleus (McGregor *et al.* 2005). Thus, trigeminal motoneurons are influenced by NO supplied by axo-terminal domains located at the TMN and not by remotely located somato-dendritic compartments. This might provide NO signaling with particular properties in the motor nucleus. Since tiny axo-terminal sources should produce much less NO than large somato-dendritic sources, they are more appropriate for fine-tuning NO release than large somas; consequently, by selectively activating individual tiny terminals, the NO signal can be targeted within a group of motoneurons. In contrast, increases in cytosolic Ca^{2+} leading to NO formation will be mediated by postsynaptic NMDA channels at somato-dendritic domains (Bredt 2003) and by presynaptic VGCCs at nitrergic terminals (Okada *et al.* 2004). Then, *in vivo*, fields of NO diffusion in clusters of motoneurons would be shaped by tuning free Ca^{2+} levels at nitrergic terminals through variations in the discharge pattern of NO-producing neurons (Park *et al.* 1998) or through the selective activation of presynaptic transmitter receptors (Okada *et al.* 2004). The latter would be performed by classical neurotransmitters synaptically released either from contiguous inputs or from the same nitrergic terminals where these neurotransmitters may colocalize with nNOS (Maqbool *et al.* 1995), such as glutamate (M. G. Fabbiani, R. McGregor, I. Pose, M. Chase and F. Morales, unpublished data; Pose *et al.* 2011a). Accordingly, NMDA increased NO content in TMN motoneurons (Fig. 6e) suggesting that presynaptic NMDA receptor-mediated Ca^{2+} influx activated nNOS to produce NO in pre-motor TMN fibers as reported in cerebellar parallel fibers (Lev-Ram *et al.* 1995).

In conclusion, we demonstrate here the ability of small sources to generate sufficient endogenous NO to recruit numerous large somas despite of the source/target size disparity and source dispersion. Our findings evidence the faculty of the nitrergic system to coordinate the activity of groups of motoneurons. This should be relevant during mastication, carrying or biting. Adjustments of intracellular Ca^{2+} by differential activation of presynaptic receptors at nitrergic terminals might be a strategy to shape the NO diffusion field extent and design patterns of NO connectivity within the TMN.

Acknowledgements

Partially funded by CSIC – Universidad de la República Oriental del Uruguay (UDELAR), Montevideo – Uruguay (to VA) and by

Programa de Desarrollo de las Ciencias Básicas (PEDECIBA) – Montevideo – Uruguay (to VA, AFA, and RB). We thank Dr A. Denicola for valuable comments, Dr J. L. Peña for his faithful support, and E. Agote, CEINBIO (Centro de Investigaciones Biomédicas), Fundación Manuel Pérez and Departamento de Histología from Facultad de Medicina – UDELAR, S. Astrada MSc. and Merial SA for technical assistance. This work is part of A. Fernández-Alvarez's doctoral project for PEDECIBA.

References

Abudara V., Fernández-Alvarez A., Chase M. H. and Morales F. R. (2002) Nitric oxide as an anterograde neurotransmitter in the trigeminal motor pool. *J. Neurophysiol.* **88**, 497–506.

Alderton W. K., Cooper C. E. and Knowles R. G. (2001) Nitric oxide synthases: structure, function and inhibition. *Biochem. J.* **357**, 593–615.

Beckman J. S. and Koppenol W. H. (1996) Nitric oxide, superoxide, and peroxynitrite: the good, the bad, and ugly. *Am. J. Physiol.*. **271**, C1424–C1437. Review.

Bindokas V. P., Jordan J., Lee C. C. and Miller R. J. (1996) Superoxide production in rat hippocampal neurons: selective imaging with hydroethidine. *J. Neurosci.* **16**, 1324–1336.

von Bohlen und Halbach O. (2003) Nitric oxide imaging in living neuronal tissues using fluorescent probes. *Nitric Oxide* **9**, 217–228.

Bredt D. S. (1999) Endogenous nitric oxide synthesis: biological functions and pathophysiology. *Free Radic. Res.* **31**, 577–596.

Bredt D. S. (2003) Nitric oxide signaling specificity – the heart of the problem. *J. Cell Sci.* **116**, 9–15.

Bredt D. S. and Snyder S. H. (1990) Isolation of nitric oxide synthetase, a calmodulin-requiring enzyme. *Proc. Natl Acad. Sci. USA* **87**, 682–685.

Bredt D. S. and Snyder S. H. (1992) Nitric oxide, a novel neuronal messenger. *Neuron* **8**, 3–11.

Broillet M., Randin O. and Chatton J. (2001) Photoactivation and calcium sensitivity of the fluorescent NO indicator 4,5-diaminofluorescein (DAF-2): implications for cellular NO imaging. *FEBS Lett.* **491**, 227–232.

Brown L. A., Key B. J. and Lovick T. A. (1999) Bio-imaging of nitric oxide-producing neurones in slices of rat brain using 4,5-diaminofluorescein. *J. Neurosci. Methods* **92**, 101–110.

Christopherson K. S., Hillier B. J., Lim W. A. and Bredt D. S. (1999) PSD-95 assembles a ternary complex with the *N*-methyl-D-aspartic acid receptor and a bivalent neuronal NO synthase PDZ domain. *J. Biol. Chem.* **274**, 27467–27473.

De Vente J., Hopkins D. A., Markerink-Van Ittersum M., Emson P. C., Schmidt H. H. and Steinbusch H. W. (1998) Distribution of nitric oxide synthase and nitric oxide-receptive, cyclic GMP-producing structures in the rat brain. *Neuroscience* **87**, 207–241.

Denicola A., Souza J. M., Radi R. and Lissi E. (1996) Nitric oxide diffusion in membranes determined by fluorescence quenching. *Arch. Biochem. Biophys.* **328**, 208–212.

Espey M. G., Thomas D. D., Miranda K. M. and Wink D. A. (2002) Focusing of nitric oxide mediated nitrosation and oxidative nitrosylation as a consequence of reaction with superoxide. *Proc. Natl Acad. Sci. USA* **99**, 11127–11132.

Furuyama T., Inagaki S. and Takagi H. (1993) Localizations of alpha 1 and beta 1 subunits of soluble guanylate cyclase in the rat brain. *Brain Res. Mol. Brain Res.* **20**, 335–344.

Garthwaite J. (2008) Concepts of neural nitric oxide-mediated transmission. *Eur. J. Neurosci.* **27**, 2783–2802.

Griffiths C., Wykes V., Bellamy T. C. and Garthwaite J. (2003) A new and simple method for delivering clamped nitric oxide concentrations in the physiological range: application to activation of guanylyl cyclase-coupled nitric oxide receptors. *Mol. Pharmacol.* **64**, 1349–1356.

Hall C. N. and Garthwaite J. (2009) What is the real physiological NO concentration in vivo? *Nitric Oxide* **21**, 92–103.

Hobbs A. J. (1997) Soluble guanylate cyclase: the forgotten sibling. *Trends Pharmacol. Sci.* **18**, 484–491.

Honig M. G. and Hume R. I. (1989) Carbocyanine dyes. Novel markers for labelling neurons. *Trends Neurosci.* **12**, 336–338.

Hope B. T., Michael G. J., Knifge K. M. and Vincent S. R. (1991) Nitric oxide synthase and neuronal NADPH-diaphorase are identical in brain and peripheral tissues. Neuronal diaphorase is a nitric oxide synthase. *Proc. Natl Acad. Sci. USA* **88**, 2811–2814.

Jourd'heuil D. (2002) Increased nitric oxide-dependent nitrosylation of 4,5-diaminofluorescein by oxidants: implications for the measurement of intracellular nitric oxide. *Free Radic. Biol. Med.* **33**, 676–684.

Kojima H., Nakatsubo N., Kikuchi K., Urano Y., Kawahara S., Kirino Y., Nagoshi H., Hirata Y. and Nagano T. (1998a) Detection and imaging of nitric oxide with novel fluorescent indicators: diaminofluoresceins. *Anal. Chem.* **70**, 2446–2453.

Kojima H., Nakatsubo N., Kikuchi K., Urano Y., Higuchi T., Tanaka J., Kudo Y. and Nagano T. (1998b) Direct evidence of NO production in rat hippocampus and cortex using a new fluorescent indicator: DAF-2 DA. *Neuroreport* **15**, 3345–3348.

Kojima H., Hirata M., Kudo Y., Kikuchi K. and Nagano T. (2001) Visualization of oxygen-concentration-dependent production of nitric oxide in rat hippocampal slices during aglycemia. *J. Neurochem.* **76**, 1404–1410.

Lancaster J. R. Jr (1997) A tutorial on the diffusibility and reactivity of free nitric oxide. *Nitric Oxide* **1**, 18–30.

Lancaster J. R. Jr (1994) Simulation of the diffusion and reaction of endogenously produced nitric oxide. *Proc. Natl Acad. Sci. USA* **91**, 8137–8141.

Ledo A., Barbosa R. M., Gerhardt G. A., Cadenas E. and Laranjinha J. (2005) Concentration dynamics of nitric oxide in rat hippocampal subregions evoked by stimulation of the NMDA glutamate receptor. *Proc. Natl Acad. Sci. USA* **102**, 17483–17488.

Leikert J. F., Rathel T. R., Muller C., Vollmar A. M. and Dirsch V. M. (2001) Reliable in vitro measurement of nitric oxide released from endothelial cells using low concentrations of the fluorescent probe 4,5-diaminofluorescein. *FEBS Lett.* **506**, 131–134.

Lev-Ram V., Makings L. R., Keitz P. F., Kao J. P. and Tsien R. Y. (1995) Long-term depression in cerebellar Purkinje neurons results from coincidence of nitric oxide and depolarization-induced Ca^{2+} transients. *Neuron* **15**, 407–415.

Maqbool A., Batten T. F. and McWilliam P. N. (1995) Co-localization of neurotransmitter immunoreactivities in putative nitric oxide synthesizing neurones of the cat brain stem. *J. Chem. Neuroanat.* **8**, 191–206.

Mariño J. and Cudeiro J. (2003) Nitric oxide-mediated cortical activation: a diffuse wake-up system. *J. Neurosci.* **23**, 4299–4307.

McGregor R., Damian A., Fabbiani G., Torterolo P., Pose I., Chase M. and Morales F. R. (2005) Direct hypothalamic innervation of the trigeminal motor nucleus: a retrograde tracer study. *Neuroscience* **136**, 1073–1081.

Mo E., Amin H., Bianco I. H. and Garthwaite J. (2004) Kinetics of a cellular nitric oxide/cGMP/phosphodiesterase-5 pathway. *J. Biol. Chem.* **279**, 26149–26158.

Moller M., Botti H., Batthyany C., Rubbo H., Radi R. and Denicola A. (2005) Direct measurement of nitric oxide and oxygen partitioning into liposomes and low density lipoprotein. *J. Biol. Chem.* **280**, 8850–8854.

Montero F., Portillo F., González-Forero D. and Moreno-López B. (2008) The nitric oxide/cyclic guanosine monophosphate pathway

modulates the inspiratory-related activity of hypoglossal motoneurons in the adult rat. *Eur. J. Neurosci.* **28**, 107–116.

Murphy S., Simmons M. L., Agullo L., Garcia A., Feinstein D. L., Galea E., Reis D. J., Minc-Golomb D. and Schwartz J. P. (1993) Synthesis of nitric oxide in CNS glial cells. *Trends Neurosci.* **16**, 323–328.

Okada D., Yap C. C., Kojima H., Kikuchi K. and Nagano T. (2004) Distinct glutamate receptors govern differential levels of nitric oxide production in a layer-specific manner in the rat cerebellar cortex. *Neuroscience* **125**, 461–472.

Park J. H., Straub V. A. and O'Shea M. (1998) Anterograde signaling by nitric oxide: characterization and in vitro reconstitution of an identified nitrergic synapse. *J. Neurosci.* **18**, 5463–5476.

Philippides A., Husbands P. and O'Shea M. (2000) Four-dimensional neuronal signaling by nitric oxide: a computational analysis. *J. Neurosci.* **20**, 1199–1207.

Philippides A., Ott S. R., Husbands P., Lovick T. A. and O'Shea M. (2005) Modeling cooperative volume signaling in a plexus of nitric oxide synthase-expressing neurons. *J. Neurosci.* **25**, 6520–6532.

Pose I., Fung S., Sampogna S., Chase M. H. and Morales F. R. (2005) Nitrergic innervation of trigeminal and hypoglossal motoneurons in the cat. *Brain Res.* **1041**, 29–37.

Pose I., Sampogna S., Chase M. H. and Morales F. R. (2011a) Nitrergic ventro-medial medullary neurons activated during cholinergically induced active (rapid eye movement) sleep in the cat. *Neuroscience* **172**, 246–255.

Pose I., Silveira V. and Morales F. R. (2011b) Inhibition of excitatory synaptic transmission in the trigeminal motor nucleus by the nitric oxide-cyclicGMP signaling pathway. *Brain Res.* **1393**, 1–16.

Rodríguez J., Specian V., Maloney R., Jourd'heuil D. and Feelisch M. (2005) Performance of diamino fluorophores for the localization of sources and targets of nitric oxide. *Free Radic. Biol. Med.* **38**, 356–368.

Schuman E. M. and Madison D. V. (1994) Locally distributed synaptic potentiation in the hippocampus. *Science* **263**, 532–536.

Shigenaga Y., Yoshida A., Tsuru K., Mitsuhiro Y., Otani K. and Cao C. Q. (1988) Physiological and morphological characteristics of cat masticatory motoneurons - intracellular injection of HRP. *Brain Res.* **461**, 238–256.

Tao H. W. and Poo M. (2001) Retrograde signaling at central synapses. *Proc. Natl Acad. Sci. USA* **98**, 11009–11015.

Uemura-Sumi M., Takahashi O., Matsushima R., Takata M., Yasui Y. and Mizuno N. (1982) Localization of masticatory motoneurons in the trigeminal motor nucleus of the guinea pig. *Neurosci. Lett.* **29**, 219–224.

Wardman P. (2007) Fluorescent and luminescent probes for measurement of oxidative and nitrosative species in cells and tissues: progress, pitfalls, and prospects. *Free Radic. Biol. Med.* **43**, 995–1022.

West A. R. and Grace A. A. (2004) The nitric oxide-guanylyl cyclase signaling pathway modulates membrane activity States and electrophysiological properties of striatal medium spiny neurons recorded in vivo. *J. Neurosci.* **24**, 1924–1935.

Wiklund N. P., Cellek S., Leone A. M., Iversen H. H., Gustafsson L. E., Brundin L., Furst V. W., Flock A. and Moncada S. (1997) Visualization of nitric oxide released by nerve stimulation. *J. Neurosci. Res.* **47**, 224–232.

Wood J. and Garthwaite J. (1994) Models of the diffusional spread of nitric oxide: implications for neural nitric oxide signaling and its pharmacological properties. *Neuropharmacology* **33**, 1235–1244.

Zhang X., Kim W. S., Hatcher N., Potgieter K., Moroz L. L., Gillette R. and Sweedler J. V. (2002) Interfering with nitric oxide measurements; 4,5-diaminofluorescein reacts with dehydroascorbic acid and ascorbic acid. *J. Biol. Chem.* **277**, 48472–48478.

Zoli M., Torri C., Ferrari R., Jansson A., Zini I., Fuxe K. and Agnati L. F. (1998) The emergence of the volume transmission concept. *Brain Res. Brain Res. Rev.* **26**, 136–147.